JTTEE5 19:81–88
DOI: 10.1007/s11666-009-9438-7
1059-9630/$19.00 © ASM International

Effect of Powder Characteristics on Properties of Warm-Sprayed WC-Co Coatings

Pornthep Chivavibul, Makoto Watanabe, Seiji Kuroda, Jin Kawakita, Masayuki Komatsu, Kazuto Sato, and Junya Kitamura

(Submitted April 24, 2009; in revised form October 2, 2009)

In high-velocity oxy-fuel (HVOF) spraying of WC-Co coatings, the decomposition and decarburization of WC during deposition are responsible for their much lower toughness compared with a sintered bulk WC-Co. In a previous study, Warm Spray (WS) process, which is capable to control the flame temperature used to propel powder particles, was successfully applied in an attempt to suppress such detrimental reactions by keeping particles' temperature lower than their melting point. The coatings deposited by WS process showed no or little formation of W_2C and η phases and demonstrated moderately improved fracture properties. However, there is still a gap in fracture toughness between WS coatings and the corresponding sintered bulk. In order to optimize the properties of the WS coatings, the effect of original powder sizes were investigated. Microstructural characterization and phase analysis were carried out on deposited coatings by SEM and XRD. The results show that the feedstock powder size has substantial effects on the properties of the coatings, i.e., the smaller powder showed improved properties.

Keywords coating, HVOF, powder size, warm spray, WC-Co

1. Introduction

WC-Co cermet coatings have been used to enhance the wear resistance of various engineering components in a variety of industrial environments. Many thermal spraying techniques such as air plasma spraying (APS) and high-velocity oxy-fuel (HVOF) spraying can be applied to deposit WC-Co coatings, however, the properties of such coatings strongly depend on the spraying technique. Compared to other spraying techniques, HVOF spraying is one of the best methods for depositing conventional WC-Co cermets, because the higher velocities and lower temperatures experienced by the powder result in less decomposition of WC during spraying process (Ref 1). Therefore, coatings with higher amount of retained WC and lower porosity are expected. However, when compared to sintered WC-Co, which has been fabricated in carefully controlled sintering condition, HVOF-sprayed WC-Co coatings suffer from decomposition and decarburization during spraying process leading to a formation of undesirable phases such as W_2C, W, and amorphous or nanocrystalline Co-W-C phase (Ref 2, 3). Many studies have shown the effect of these phases on the properties of the coating (Ref 3-7). Chivavibul et al. (Ref 5) systematically studied the effects of both carbide size and Co content on the mechanical properties of the coatings. It was found that the hardness and fracture resistance of the coatings were different from those of the sintered WC-Co. This discrepancy could be mainly explained by the hardening of the binder phase due to the dissolution of WC and the formation of amorphous/nanocrystalline phases. The hardness of the binder phase estimated from the experimental data using the mixing rule ranged from 1000 to 1300 Hv, which was quite higher than those of the binder phase in the sintered WC-Co (490-660 Hv).

Many efforts have been made to deposit WC-Co coating in lower temperature ranges than those of HVOF process in order to suppress decarburization and decomposition of WC phases by using high-velocity air fuel (HVAF), cold spray, pulsed gas dynamic spraying (PGDS), and Warm spray (WS) processes (Ref 8-18). These coatings show no/little detrimental phase transformation and decarburization of WC. Therefore, it indicates the capability to fabricate WC-Co coatings, which have

This article is an invited paper selected from presentations at the 2009 International Thermal Spray Conference and has been expanded from the original presentation. It is simultaneously published in *Expanding Thermal Spray Performance to New Markets and Applications: Proceedings of the 2009 International Thermal Spray Conference*, Las Vegas, Nevada, USA, May 4-7, 2009, Basil R. Marple, Margaret M. Hyland, Yuk-Chiu Lau, Chang-Jiu Li, Rogerio S. Lima, and Ghislain Montavon, Ed., ASM International, Materials Park, OH, 2009.

Pornthep Chivavibul, Makoto Watanabe, Seiji Kuroda, Jin Kawakita, and **Masayuki Komatsu**, Composites and Coatings Center, National Institute for Materials Science, Ibaraki, Japan; and **Kazuto Sato** and **Junya Kitamura**, Fujimi Incorporated, Gifu, Japan. Contact e-mail: CHIVAVIBUL.Pornthep@nims.go.jp.

the similar microstructure as the sintered materials. Recently, Chivavibul et al. (Ref 8) comparatively studied the properties of WC-Co coatings with different Co contents that were deposited from both HVOF and WS processes. It was found that the hardness of WS coatings were lower than those of HVOF coatings, but the hardness-Co content relation in WS coatings was similar to that in sintered materials. WS showed improvement in fracture resistance compared with conventional HVOF but there still exists a gap from a sintered bulk. Further systematic study of this process, therefore, is still required for the application of this new process.

In the present investigation, the effect of original powder size on the properties of WS coating is studied. Nano-sized WC-Co powders with various Co contents and powder size ranges are sprayed by the WS techniques. Phase distribution and microstructure of the coating are examined by x-ray diffraction and scanning electron microscope (SEM), respectively. Hardness, fracture toughness, and erosion wear properties are measured. The relation between the microstructural features and the mechanical properties of the WS coatings are discussed based on experimental results.

2. Experimental Procedure

2.1 Materials and Spraying Process

Six WC-Co powders with an average carbide sizes of 0.2 μm and different cobalt contents (12, 17, and 25 wt.%) and particle size ranges ($-45+15$ and $-20+5$ μm) were used in this work. The powders were manufactured by spray drying of slurries containing WC and Co particles, followed by light sintering, crushing, and classification. Examples of cross section of WC-12Co powders with different particle size ranges are shown in Fig. 1. All powders have typically spherical shape with some amounts of pores distributing in the cross sections.

The WS process was developed by adding a mixing chamber to introduce nitrogen gas between the combustion chamber and powder feed port of the commercial HVOF equipment (JP5000, Praxair Technology Inc., Danbury, CT). Details of the spraying equipment were given elsewhere (Ref 8, 19). Carbon steel substrates (0.45%C) were used. Table 1 shows the spraying conditions of WS process. The thickness of coatings was approximately 300 μm. For convenience, the coatings deposited from $-45+15$ to $-20+5$ μm powders were labeled C (coarse) and F (fine), respectively, with the number after the character showing Co content.

2.2 Coating Characterization

X-ray diffraction (XRD) was conducted for the powders and as-fabricated coatings with the Cu Kα radiation at 40 kV and 300 mA. Cross sections of the coatings were obtained by embedding specimens in cold mounting resin followed by grinding and polishing to a 1 μm finish and examined by scanning electron microscopy (SEM). Some coatings' sections were also prepared by the cross section polisher (CP), which utilizes an argon ion beam to mill the sample. This method prevents

Table 1 Spray condition for WC-Co coatings

	WS
Barrel length, mm	203
Spraying distance, mm	200
Fuel, l/min	0.38
Oxygen, l/min	778
Nitrogen, 1/min	500
Powder feed rate, g/min	80
Powder feed gas	Nitrogen

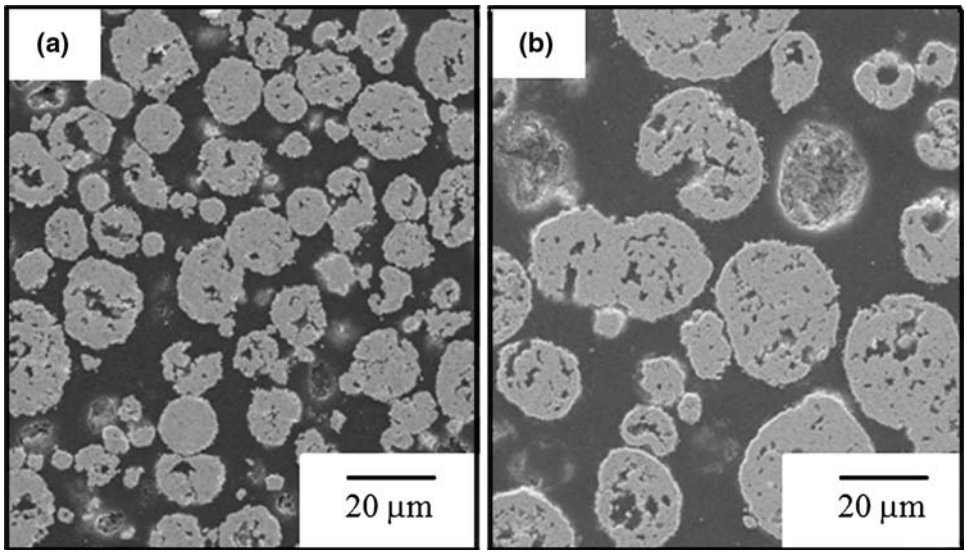

Fig. 1 SE images of cross sections of WC-12Co powders: (a) $-20+5$ μm and (b) $-45+15$ μm

Table 2 Erosion conditions

Erodent material	Alumina
Average particle size, μm	500
Particle shape	Angular
Air pressure, MPa	0.4
Nozzle distance, mm	50
Impact angle	30, 90

any plastic deformation of Co phase that occurs during the mechanical polishing and therefore can provide a real microstructure of the coatings. The porosity of the coatings was determined by mercury intrusion porosimetry (Micromeritics Autopore II 9220).

Microhardness tests were carried out with a 300 g load and a dwell time of 15 s. At least ten measurements were made for each sample. The fracture toughness of the coatings was determined by the indentation method with a 10 kg load and a dwell time of 15 s. Both the crack lengths and Vickers diagonals were measured by an optical microscope. The fracture resistance, K_C, was determined under an assumption that the cracks generated from an indentation were radial cracks possessing the Palmqvist geometry by the following equation (Ref 20):

$$K_C = 0.0193(H_v D)\left(\frac{E}{H_v}\right)^{2/5}(a)^{-1/2} \quad \text{(Eq 1)}$$

where H_v is the Vickers hardness, E is the Young's modulus, D is the half-diagonal of the Vickers indentation, and a is the indentation crack length. At least five indentations were made for each sample. The Young's modulus of the coatings was assumed to be 300 GPa for all the samples.

Erosion resistance of the coatings was evaluated using a blast erosion tester with the test conditions listed in Table 2. Tests were performed up to three runs for each specimen. The average weight losses of all the samples were converted to volume losses by using the density values of the sintered materials and then normalized with that of the JIS-SS400 low carbon steel.

3. Results and Discussion

3.1 Coating Microstructure

Examples of secondary electron (SE) and back scattered electron (BE) images of WS coatings are shown in Fig. 2. The low magnification images of C17 and F17 are shown in Fig. 2(a) and (b), respectively. Both images revealed dense coatings with a thickness of approximately 300 μm. The coating deposited from the smaller powder showed an improvement (decrease) of surface roughness as can be seen in Fig. 2(b). Higher magnification images (Fig. 2c, d) are showing densely packed fine carbide in binder phase. Some amount of pores was observed in both of the coatings. In some area, lacks of splat-splat bonding were also observed. Compared with HVOF process, by which the deposition with small powder (~10 μm) is difficult due to the spitting problem, WS process could produce coatings using such fine powder because the deposition is carried out essentially in the solid state. The improvement of surface roughness is beneficial for post-spray polishing process because the time and cost for grinding and polishing can be reduced.

Examples of XRD patterns of C- and F-series coatings are shown in Fig. 3(a) and (b), respectively. The results of WC-12Co powder is also given for comparison. Both C- and F-series coatings showed the peaks of WC and Co phase like the feedstock powder for all the Co contents, but a small peak of W_2C was observed in F12 coating. This indicates that little composition and phase changes took place during the deposition. Moreover, there were two points to be noted. The first was that WC peaks of WS coatings were broadened comparing to those of the powder. The other was that Co peaks of WS coatings were also broadened and shifted to lower angles. Possible explanations for these findings are the deformation of WC and Co phases due to high-velocity impact of powder during deposition and dissolution of WC into the Co phase (Ref 8).

A plot of porosity measured by mercury intrusion porosimeter as a function of Co content is shown in Fig. 4. The data of F25 are absent because the measurement was failed and there was a limitation of sample. It should be noted that the data presented in this figure are the values of open pores only; close pores cannot be measured by mercury intrusion porosimeter. The porosity decreased with increasing Co contents for C-series coating, while the porosity is approximately 0.6 vol.% for F-series-coatings. This means that reducing the powder size is very effective to lower defects in the WS coating.

3.2 Mechanical Properties of the Coating

3.2.1 Hardness and Fracture Resistance. The microhardness and fracture toughness values of the HVOF and WS coatings as a function of Co content are shown in Fig. 5. The values of the sintered materials (Ref 8) and HVOF coatings (Ref 5) are also given for a comparison. The WS coatings had lower hardness values than those of the sintered ones for all the Co contents, however, a trend of hardness reduction with Co content was the same. In contrast, the hardness of HVOF coatings only slightly changed with Co content. These are related to the different phase distribution between WS and HVOF coatings as previously reported by Chivavibul et al. (Ref 8). F-series coatings showed higher hardness values than C-series coating by about 100 Hv for all the Co contents. A possible explanation for this behavior is attributed to the reduction of porosity in F-series as shown in Fig. 4. Although the value of close pores could not be detected by mercury porosimeter, it clearly revealed that coating integrity can be improved with smaller powder. The other explanation for hardness increment might be due to the improvement of splat-splat bonding. Figure 6 shows SEM photographs of cross section of C12 and F12 coatings prepared by the cross section polisher. Vertical white lines in Fig. 6(a) are scratched due to an ion beam. The pores are highlighted due to the edge effects in the SE mode,

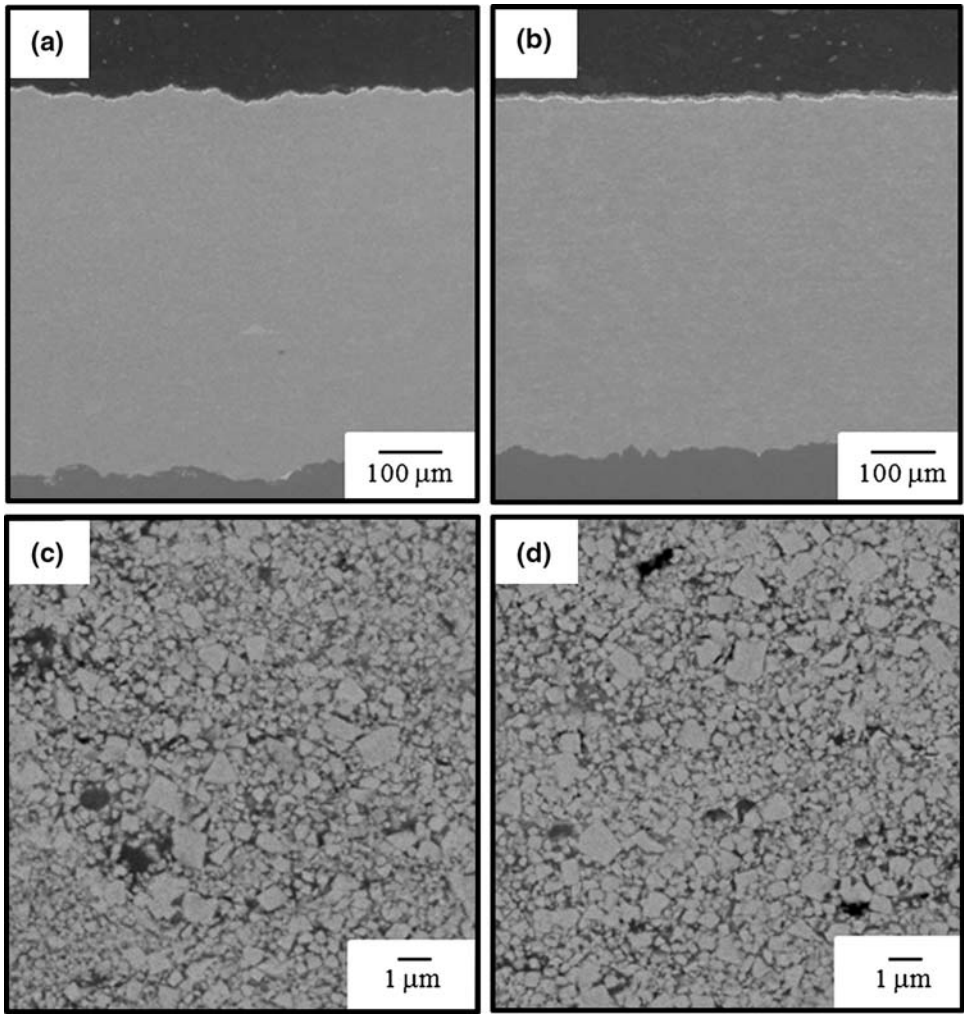

Fig. 2 Observation of (a) C17 and (b) F17 coatings in SE mode. Higher magnifications are shown in (c) and (d) in BE mode, respectively

revealing the morphologies and distribution of them. Compared to the cross sections prepared by mechanical polishing as shown in Fig. 2(c) and (d), defects such as pores and lack of splat-splat bonding could be more clearly identified in Fig. 6 because no plastic deformation of Co phase occurred during sample preparation, which could cover defects or change the shape of defects. Both coatings are showing a number of small pores. These pores are located likely along a line parallel to the coating-substrate interface shown by the marked zones in Fig. 6. Furthermore, crack-like defects running horizontally are observed in C12 coatings indicated by arrows in Fig. 6(a). Higher magnification of these defects is shown in Fig. 6(b). These areas are probably splat-splat interfaces. Although it is not quantitative, amount of defects in splat-splat area in F12 coating is less than that in C12 coating. Therefore, one can infer that using smaller powder size provides the improvement of splat-splat bonding. The image analysis was applied to measured the porosity on cross section micrographs (5k× magnification) prepared by CP. The porosity values of C12 and F12 were 2.2 ± 0.2 and $1.7 \pm 0.3\%$, respectively, while those measured by porosimeter were 1.7 and 0.6%, respectively. This discrepancy is related to the close pores because the porosimeter can measure only the open pores.

The fracture resistance of WS coatings showed a tendency to increase with increasing Co contents, however, the increment was not as large as that of sintered WC-Co. The fracture resistance of both C- and F-series coatings ranged from 4 to 6 MPa $m^{1/2}$. In HVOF, the fracture resistance reduced as Co content increases probably due to embrittlement of binder phases. As mentioned above, reducing powder size lowered defects and enhanced splat-splat bonding in the WS coating leading to the increase of hardness, however, no improvement was recognized in terms of fracture resistance. SEM observations of crack path generated from indentation in C12 and F12 coatings are shown in Fig. 7. Cracks in F12 coating tended to run straightly in the direction parallel to lamellae (Fig. 7b). Cracks in C12 coating also ran in the direction parallel to

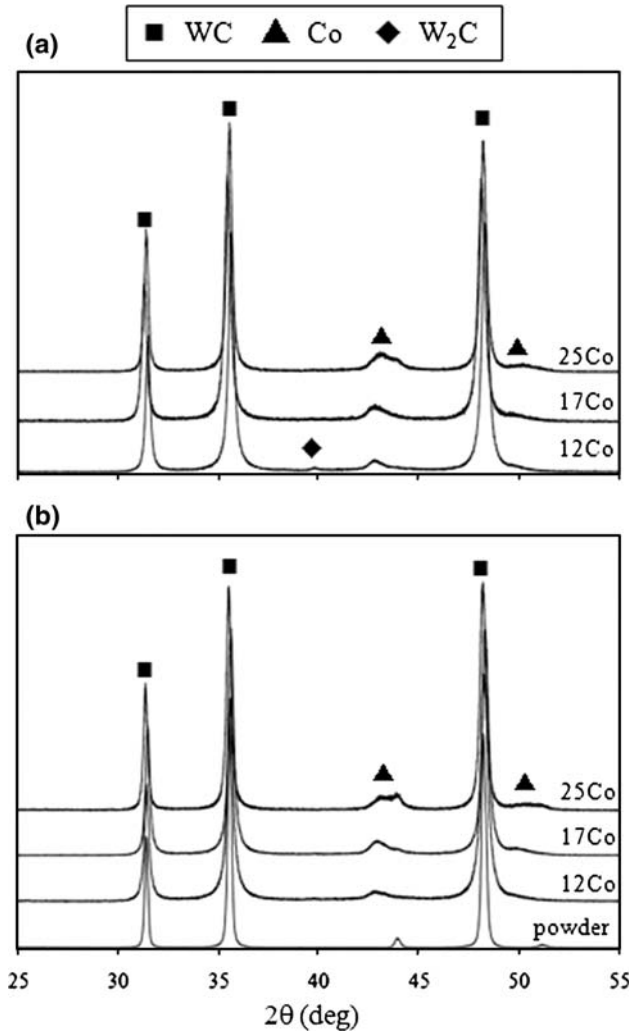

Fig. 3 XRD results of (a) F- and (b) C-series coatings. The result of WC-12Co powder is given for a comparison

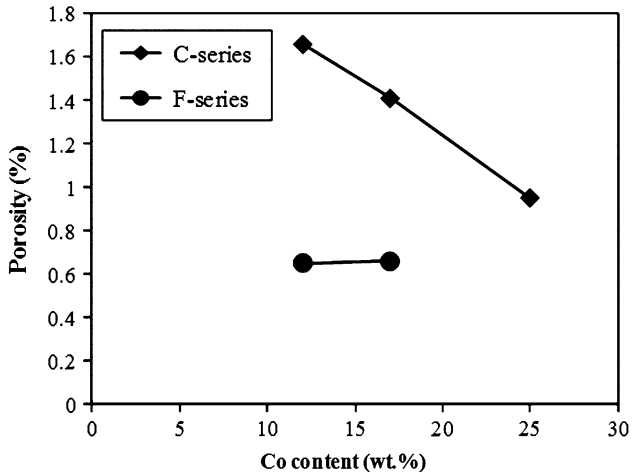

Fig. 4 Porosity of WS coatings as a function of Co content

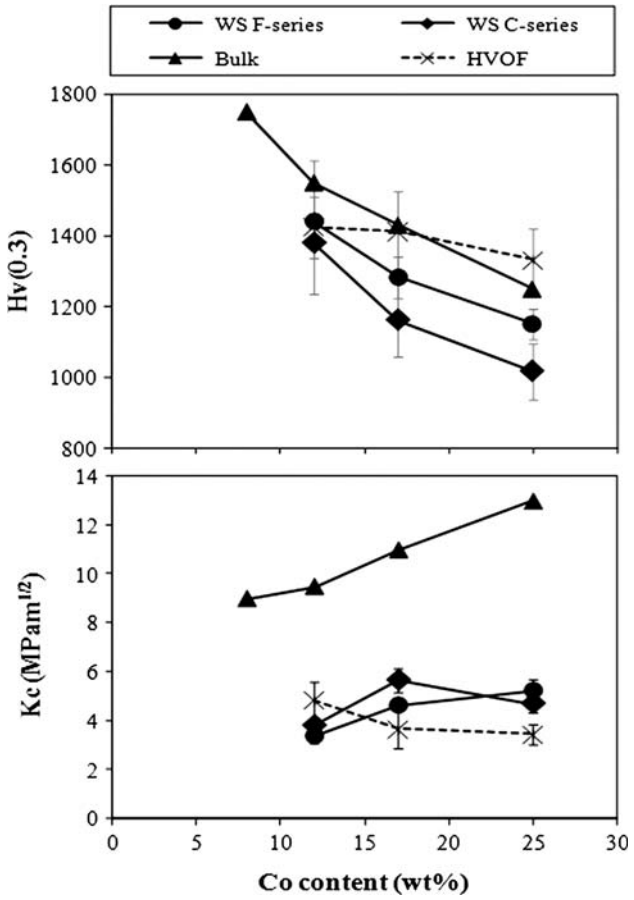

Fig. 5 (a) Hardness and (b) fracture resistance as a function of cobalt content

lamellae but their shape are wavier than those in F12 coating. Since the splat-splat boundaries are considered to be the weakest links in the coating, it is likely that the crack propagated along the splat-splat boundaries. It is reasonable, therefore, that the cracks in C12 coating are wavier than those in F12 because the size of the feedstock powder of C12 is coarser than F12. In order to obtain high quality WS coatings, it is expected that sprayed powder particles attain sufficiently high temperature and velocity so that the powder can deform well at the impact onto the substrate or the coating surface to densify the coating and to achieve intimate splat-splat bonding. Even though particles acceleration and heating in a thermal spraying apparatus and the deceleration and cooling during flight in the environment are not a simple phenomenon, it has been generally shown that smaller particles tend to be heated and accelerated more quickly to a higher temperature and velocity. If such more energetic state of finer powder is retained to the point of impact at the substrate position, it can play a role in achieving a better inter-splat bonding and denser coating microstructure.

3.2.2 Erosion Behavior. Erosion wear property of C- and F-series coatings as a function of Co contents is shown in Fig. 8. The data are presented in terms of the volume wear ratio, which is the volume loss of a coating

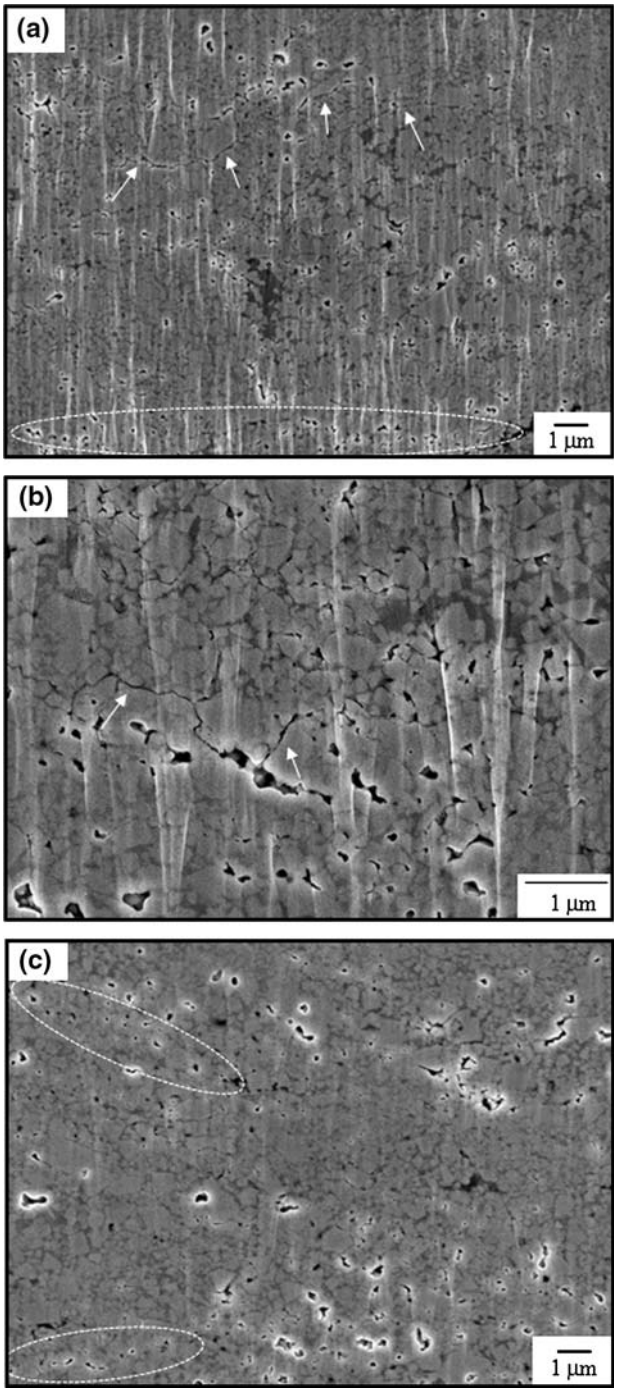

Fig. 6 SE images of specimens prepared by cross section polisher: (a) C12 coating, (b) higher magnification of the lack of bonding area in C12 coating, and (c) F12 coatings

normalized by that of a low carbon steel (JIS-SS400). Solid and dashed lines represent the results obtained from impact angles of 30° and 90°, respectively. It clearly shows that the volume losses at 90° impact angle were higher than those at 30° for all Co contents, which is a typical erosion characteristic of brittle materials. The coatings' performance is actually inferior to the carbon steel at 90°.

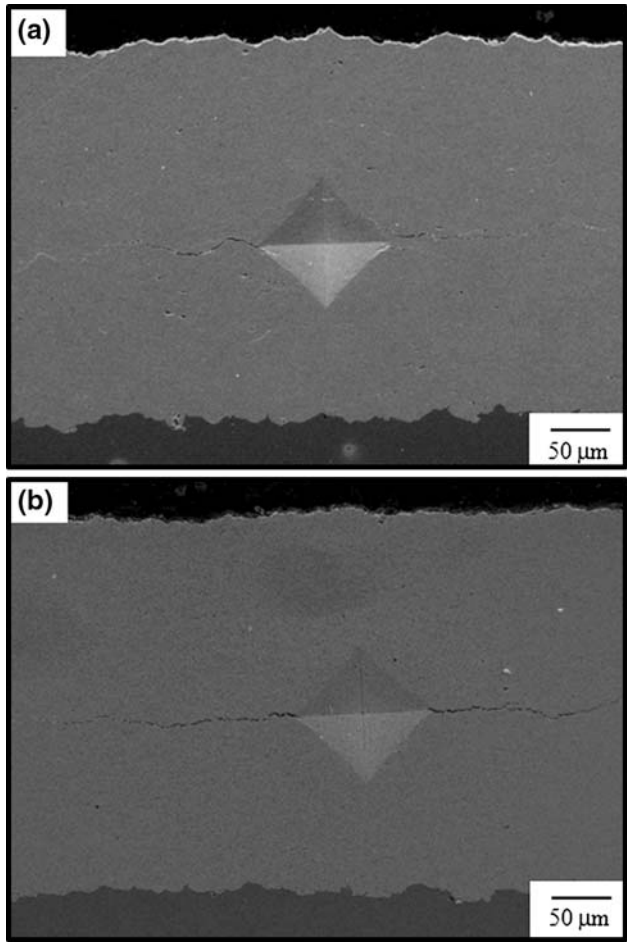

Fig. 7 Crack paths generated from indentation testing in (a) C12 and (b) F12 coatings

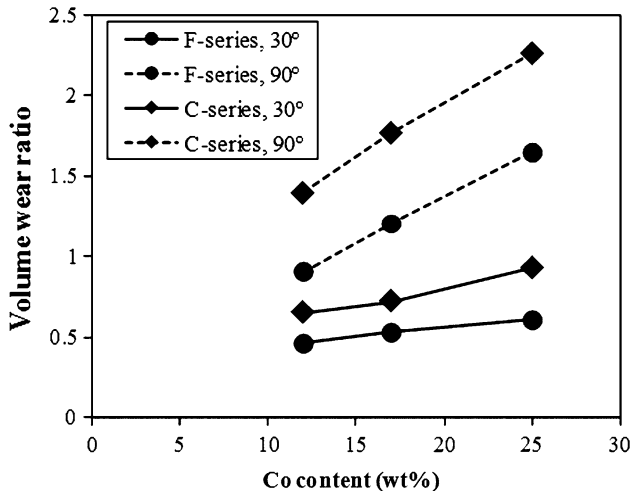

Fig. 8 Erosion wear rate as a function of Co content

The volume wear ratio tended to linearly increased with increasing Co content for both 30° and 90° impact angles and F-series coatings showed less volume loss than

C-series coatings. Figure 9 shows SEM micrographs of the surface morphology of the C12 and F12 coatings eroded at 90°. Observation at low magnification (Fig. 9a, b) showed that erosion in both C12 and F12 coatings consisted of numerous ductile cuttings formed by ploughing of erodent particle. Most cuttings were smooth, which indicated that the erodent particles cut through the WC particles as well as through the binder. However, cuttings in C12 coating were deeper than those in F12 coating. In some areas, craters as shown by dashed circles were also observed. Observation of C12 coating at higher magnification (Fig. 9c) shows some pores, pits, and cracks in the ductile cuttings as indicated by the arrows. The morphology of the pits suggests that it was caused by the removal of materials from a weak interface. As discussed previously, the microstructure of C12 sample contains many crack-like defects along the splat-splat boundary (Fig. 6a), therefore, one can infer that this interface was a splat boundary and the pit was formed by the lifting of a poorly bonded splat fragment. These were rarely observed in F12 coating (Fig. 9d), only amount of small craters formed by carbide pull out are observed. Figure 9(e) and (f) shows cross sections of eroded C12 and F12, respectively. The impact of erodent particles resulting in a formation of crack beneath the coating surface and spalling of coating was evident. These cracks mostly run parallel to the coating surface, which means that the bonding in the lamellar direction was weak. One can note that cracks in C12 coating were generated at a deeper distance from the coating surface compared to those observed in F12 coating.

Previous studies (Ref 21-23) about erosion of thermal sprayed cermet coatings described the erosion mechanism as follows. The first is microcutting and microploughing of the soft binder by hard erodent particles. With progress of erosion, the carbide particles are exposed and then gouged by the impact of erodent particles and cause further

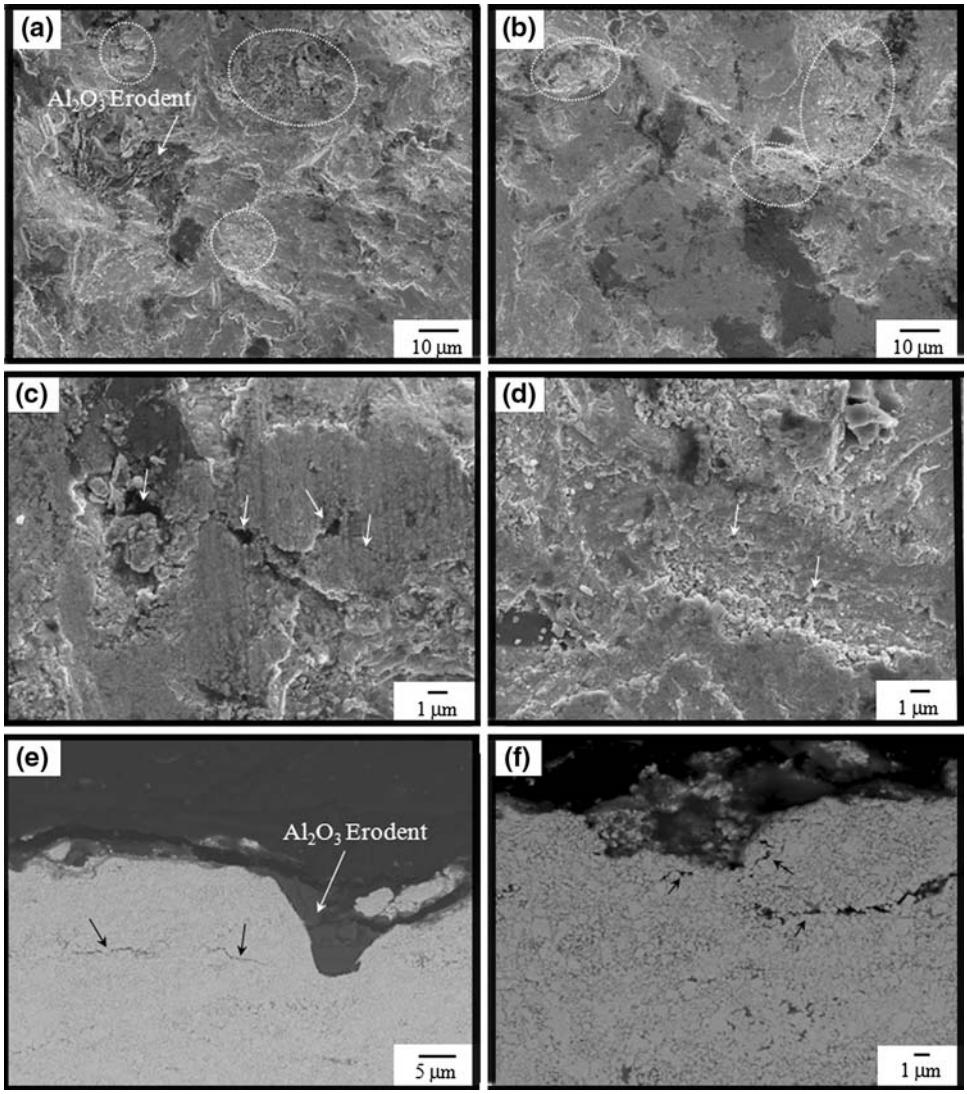

Fig. 9 Observation of C12 (a, c, and e) and F12 (b, d, and f) coatings eroded at 90°: (a) and (b) surface morphology, (c) and (d) higher magnification, (e) and (f) cross sections in BE mode

cutting. The second is the spalling of the coating due to crack propagation. The latter is considered to be a dominant mechanism for thermal sprayed cermet coatings. According to the observation of erosion wear morphology, the main erosion mechanism of the WS WC-Co coatings is also the latter one. The degree of spalling in the F-series coatings was considered to be lower than those in C-series coatings. The improvement in wear properties in F-series coating was attributed to the improvement of splat-splat bonding and reduction in porosity.

4. Conclusions

WC-Co coatings with 0.2 μm carbide size and different Co contents were deposited by warm sprayings from two different powder sizes. The microstructure, hardness, fracture resistance, and wear property of the coatings were investigated.

Characterization of the coatings revealed that coating deposited from both coarse and fine powder sizes had the phase composition essentially same as the feedstock powder, i.e., only a trace amount of W_2C peak was observed in the XRD spectrum of WC-12Co coating deposited from fine powder size. The porosity values of the coating deposited from coarse powders were higher than those deposited from the finer one. Observation of cross sections prepared by cross section polisher also revealed higher amount of pores and lack of splat-splat cohesions in the coating deposited from the coarse powders. The improvement in coating integrity resulted in the increase of hardness and improvement of wear property of the coating deposited with fine powder.

References

1. V.V. Sobolev, J.M. Guilemany, and J. Nutting, *High Velocity Oxy-Fuel Spraying*, Maney Publishing, 2004
2. J.M. Guilemany, J.M. de Paco, J. Nutting, and J.R. Miguel, Characterization of the W2C Phase Formed During the High Velocity Oxygen Fuel Spraying of a WC + 12 pct Co Powder, *Metal. Mater. Trans. A*, 1999, **30**(8), p 1913-1921
3. C. Verdon, A. Karimi, and J.L. Martin, A Study of High Velocity Oxy-Fuel Thermally Sprayed Tungsten Carbide Based Coatings. Part 1: Microstructures, *Mater. Sci. Eng. A*, 1998, **246** (1-2), p 11-24
4. Y. Ishikawa, J. Kawakita, S. Sawa, T. Itsukaichi, Y. Sakamoto, M. Takaya, and S. Kuroda, Evaluation of Corrosion and Wear Resistance of Hard Cermet Coatings Sprayed by Using an Improved HVOF Process, *J. Therm. Spray Technol.*, 2005, **14**(3), p 384-390
5. P. Chivavibul, M. Watanabe, S. Kuroda, and K. Shinoda, Effects of Carbide Size and Co Content on the Microstructure and Mechanical Properties if HVOF-Sprayed WC-Co Coatings, *Surf. Coat. Technol.*, 2007, **202**(3), p 509-521
6. M. Watanabe, A. Owada, S. Kuroda, and Y. Gotoh, Effect of WC Size on Interface Fracture Toughness of WC-Co HVOF Sprayed Coatings, *Surf. Coat. Technol.*, 2006, **201**(3-4), p 619-627
7. Y. Ishikawa, S. Kuroda, J. Kawakita, Y. Sakamoto, and M. Takaya, Sliding Wear Properties of HVOF Sprayed WC-20%Cr3C2-7%Ni Cermet Coatings, *Surf. Coat. Technol.*, 2007, **201**(8), p 4718-4727
8. P. Chivavibul, M. Watanabe, S. Kuroda, J. Kawakita, M. Komatsu, K. Sato, and J. Kitamura, Development of WC-Co Coatings Deposited by Warm Spray Process, *J. Therm. Spray Technol.*, 2008, **17**(5-6), p 750-756
9. R.S. Lima, J. Karthikeyan, C.M. Kay, J. Lindemann, and C.C. Berndt, Microstructural Characteristics of Cold-Sprayed Nanostructured WC-Co Coatings, *Thin Solid Films*, 2002, **416**(1-2), p 129-135
10. H.J. Kim, C.H. Lee, and S.Y. Hwang, Superhard Nano WC-12%Co Coating by Cold Spray Deposition, *Mater. Sci. Eng. A*, 2005, **391**(1-2), p 243-248
11. H.J. Kim, C.H. Lee, and S.Y. Hwang, Fabrication of WC-Co Coatings by Cold Spray Deposition, *Surf. Coat. Technol.*, 2005, **191**(2-3), p 335-340
12. M. Watanabe, C. Pornthep, S. Kuroda, J. Kawakita, J. Kitamura, and K. Sato, Development of WC-Co Coatings by Warm Spray Deposition for Resource Savings of Tungsten, *J. Jpn. Inst. Metals*, 2007, **71**, p 853-859
13. C.J. Li, G.J. Yang, P.H. Gao, J. Ma, Y.Y. Wang, and C.X. Li, Characterization of Nanostructured WC-Co Deposited by Cold Spraying, *J. Therm. Spray Technol.*, 2007, **16**, p 1011-1020
14. S. Kuroda, J. Kawakita, M. Watanabe, and H. Katanoda, Warm Spraying—A Novel Coating Process Based on High-Velocity Impact of Solid Particles, *Sci. Technol. Adv. Mater.*, 2008, **9**(3), p 033002 (17 pp)
15. L. Jacobs, M.M. Hyland, and M. De Bonte, Comparative Study of WC-Cermet Coatings Sprayed via the HVOF and the HVAF Process, *J. Therm. Spray Technol.*, 1998, **7**(2), p 213-218
16. L. Jacobs, M.M. Hyland, and M. De Bonte, Study of the Influence of Microstructural Properties on the Sliding-Wear Behavior of HVOF and HVAF Sprayed WC-Cermet Coatings, *J. Therm. Spray Technol.*, 1999, **8**(1), p 125-132
17. M. Yandouzi, L. Ajdelsztajn, and B. Jodoin, WC-based Composite Coatings Prepared by the Pulsed Gas Dynamic Spraying Process: Effect of the Feedstock Powders, *Surf. Coat. Technol.*, 2008, **202**(16), p 3866-3877
18. M. Yandouzi, E. Sansoucy, L. Ajdelsztajn, and B. Jodoin, WC-based Cermet Coatings Produced by Cold Gas Dynamic and Pulsed Gas Dynamic Spraying Processes, *Surf. Coat. Technol.*, 2007, **202**(2), p 382-390
19. J. Kawakita, S. Kuroda, T. Fukushima, H. Katanoda, K. Matsuo, and H. Fukanuma, Dense Titanium Coatings by Modified HVOF Spraying, *Surf. Coat. Technol.*, 2006, **201**(3-4), p 1250-1255
20. K. Niihara, A Fracture-Mechanics Analysis of Indentation-Induced Palmqvist Crack in Ceramics, *J. Mater. Sci. Lett.*, 1983, **2**(5), p 221-223
21. J. Barber, B.G. Mellor, and R.J.K. Wood, The Development of Sub-surface Damage During High Energy Solid Particle Erosion of a Thermally Sprayed WC-Co-Cr Coating, *Wear*, 2005, **259**(1-6), p 125-134
22. J.K.N. Murthy, D.S. Rao, and B. Venkataraman, Effect of Grinding on the Erosion Behaviour of a WC-Co-Cr Coating Deposited by HVOF and Detonation Gun Spray Processes, *Wear*, 2001, **249**(7), p 592-600
23. G.C. Ji, C.J. Li, Y.Y. Wang, and W.Y. Li, Erosion Performance of HVOF-Sprayed Cr_3C_2-NiCr Coatings, *J. Therm. Spray Technol.*, 2007, **16**(4), p 557-565